Carbon Dioxide Fixation | Hot Paper

Deutsche Ausgabe: DOI: 10.1002/ange.201506062
Internationale Ausgabe: DOI: 10.1002/anie.201506062

Nitrogen-Doped Carbon Nanotube Arrays for High-Efficiency Electrochemical Reduction of CO_2: On the Understanding of Defects, Defect Density, and Selectivity

Pranav P. Sharma, Jingjie Wu, Ram Manohar Yadav, Mingjie Liu, Christopher J. Wright, Chandra Sekhar Tiwary, Boris I. Yakobson, Jun Lou, Pulickel M. Ajayan,* and Xiao-Dong Zhou**

Abstract: *Nitrogen-doped carbon nanotubes (NCNTs) have been considered as a promising electrocatalyst for carbon-dioxide-reduction reactions, but two fundamental chemistry questions remain obscure: 1) What are the active centers with respect to various defect species and 2) what is the role of defect density on the selectivity of NCNTs? The aim of this work is to address these questions. The catalytic activity of NCNTs depends on the structural nature of nitrogen in CNTs and defect density. Comparing with pristine CNTs, the presence of graphitic and pyridinic nitrogen significantly decreases the overpotential (ca. −0.18 V) and increases the selectivity (ca. 80 %) towards the formation of CO. The experimental results are in congruent with DFT calculations, which show that pyridinic defects retain a lone pair of electrons that are capable of binding CO_2. However, for graphitic-like nitrogen, electrons are located in the π^* antibonding orbital, making them less accessible for CO_2 binding.*

A recent report by an international team led by Pierre Friedlingstein[1] estimated that global CO_2 discharge from fossil fuel combustion and cement production would continuously rise in 2014 to a level of about 65 % above emissions in 1990, the base year adopted in the Kyoto Protocol. Meanwhile, the daily mean concentration of carbon dioxide in the atmosphere measured at the Mauna Loa Observatory in Hawaii was recorded above 400 parts per million for the first time on May 9th, 2013. The rapid increase in CO_2 in ambient air may cause irreversible damage, resulting in an uninhabitable planet for future generations. A carbon-neutral cycle, if realized, can potentially address these issues by capturing and converting CO_2 to various liquids or gaseous fuels when coupled together with renewable energy sources.[2] The main hurdle for this technology is the availability of efficient and robust catalysts that can catalyze the multiple proton–electron transfer reactions involved in CO_2 reduction.[3] Presently, metallic electrocatalysts including Sn, Cu, Au, and Ag have been extensively investigated. However, high overpotentials, poor stability, and inferior selectivity remain major challenges yet to be tackled.[4]

Nitrogen-doped carbon nanotubes (NCNTs) have gained much attention as electrocatalysts for the oxygen-reduction reaction (ORR) and oxygen-evolution reaction (OER) because of their unique electronic[5] and geometric features.[5,6] The catalytic activity most likely originates from the nitrogen defects in the hexagonal graphitic network.[7] Unlike the ORR, reports of the application of NCNTs as catalysts for the electrochemical reduction of CO_2 are limited. Direct conversion of CO_2 to CO using a nitrogen-doped carbon nanofiber catalyst[8] in an ionic-liquid-based environment were reported, with the ionic liquid acting as a possible co-catalyst.[9] In addition to the unknown reaction mechanism in doped carbon fibers, the high costs of ionic liquids make this approach economically challenging. NCNTs have also been employed for CO_2 reduction to formate using polyethyleimine as a co-catalyst, stabilizing the CO_2^{-}* intermediate.[10] However, high overpotentials (higher than 0.6 V) were needed to catalyze this reaction. Recently, we demonstrated the superior catalytic activity of NCNTs to noble-metal catalysts, including Ag and Au, towards CO formation.[11] Here, we report our extensive study on the role of different NCNT nitrogen functionalities, that is, graphitic, pyridinic and pyrrolic nitrogen sites, on the direct conversion of CO_2 to CO without the use of a metal catalyst.

Initial research focused on tuning the nitrogen-bonding configuration and content in CNTs by using three different precursors: acetonitrile (ACN), dimethlyformamide (DMF), and triethylamine (TEA), and various growth temperatures: 750, 850, and 950 °C. Figure 1 a and b show the representative SEM images of as-synthesized NCNTs indicating the formation of well-aligned NCNT arrays with an average length about 100 μm. The TEM image (Figure 1 c) shows the bamboo-shaped morphology and multi-walled nature of the synthesized NCNTs. The bamboo-like structure is a characteristic feature of resident nitrogen atom defects in CNTs, which originates from the formation of a positive curvature surface during substitution of nitrogen atoms into the graphitic structure.[12] The local disorder and crystallinity were studied using Raman spectroscopy. Figure 1 d shows the characteristic

[*] P. P. Sharma,[+] C. J. Wright, Prof. X.-D. Zhou
Department of Chemical Engineering
University of South Carolina
Columbia, SC 29208 (USA)
E-mail: zhox@cec.sc.edu
Dr. J. Wu,[+] Dr. R. M. Yadav,[+] M. Liu, Dr. C. S. Tiwary,
Prof. B. I. Yakobson, Prof. J. Lou, Prof. P. M. Ajayan
Department of Materials Science and NanoEngineering
Rice University Houston, TX 77005 (USA)
E-mail: jlou@rice.edu
ajayan@rice.edu
[+] These authors contributed equally to this work.

Supporting information for this article is available on the WWW under http://dx.doi.org/10.1002/anie.201506062.

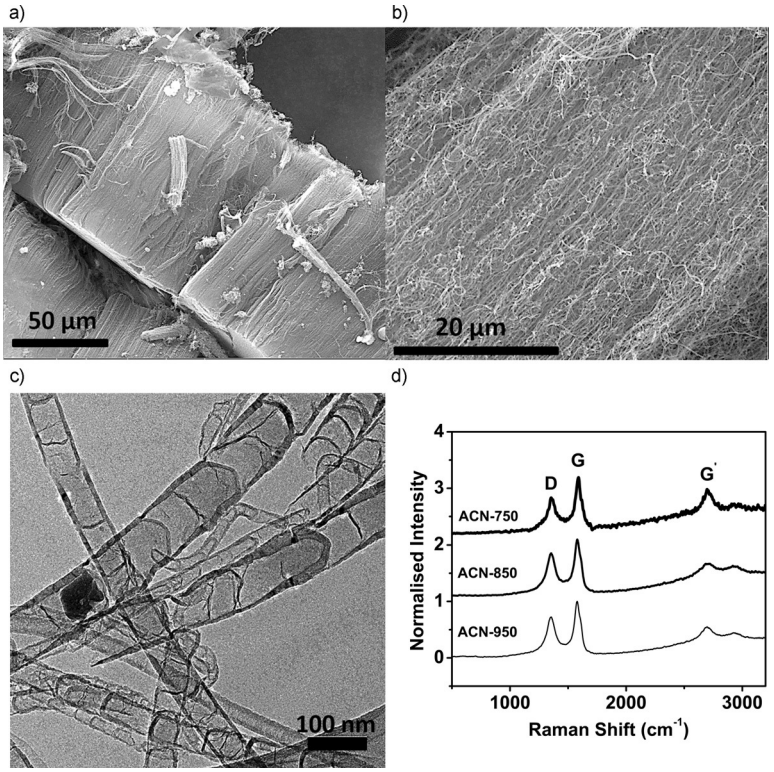

Figure 1. Physical characterization of as-synthesized NCNTs. a,b) Cross-sectional SEM images, c) TEM image, and d) Raman spectra of NCNTs synthesized using an ACN precursor at various temperatures.

D and G bands found in graphitic materials at about 1400 and 1600 cm^{-1}, respectively. The D band arises from the disordered sp^2 hybridized carbon, while G band is associated with the C–C tangential stretching mode and indicates the presence of crystalline graphitic carbon.[7c] The D- to G-band intensity ratio (I_D/I_G) is sensitive to structural defects, increasing with higher nitrogen content. The full-width-at-half-maximum (FWHM), however, depends on both structural defects[7c] and tube diameter.[13] The analyzed results are tabulated in Table 1, which shows the trends in I_D/I_G, $FWHM_D/FWHM_G$, diameter, and total N content of the NCNTs synthesized in this work.[14] The NCNTs synthesized using the ACN precursor at 850 °C (NCNTs-ACN-850) exhibited the highest I_D/I_G ratio because of the maximum nitrogen content. A further increase in temperature from 850 to 950 °C resulted in a decrease in nitrogen content from 4.9 to 3.9 at % (Table 1) possibly due to the formation of nitrogen molecules.[15] The diameter of NCNTs depends upon nitrogen content, which in turn is influenced by synthesis conditions.[15] The $FWHM_D/FWHM_G$ ratio, however, decreased with increasing tube diameter and total nitrogen content, accounting for both structural defect density and curvature-induced strain in the NCNTs.[13]

Table 1: Trends in diameter, I_D/I_G, $FWHM_D/FWHM_G$, and total nitrogen content of different NCNTs synthesized using various precursors. ACN-750, ACN-850, and ACN-950 represent the NCNTs synthesized using the ACN precursor at 750, 850, and 950 °C, respectively. DMF-850 and TEA-850 denote the NCNTs synthesized using DMF and TEA precursors, respectively, at 850 °C.[14]

NCNTs	Diameter [nm]	I_D/I_G	$FWHM_D/FWHM_G$	Total nitrogen content [at %]
ACN-750	55	0.64	1.63	1.9
ACN-850	66	0.78	1.34	4.9
ACN-950	75	0.72	1.47	3.9
DMF-850	45	0.62	1.34	2.8
TEA-850	31	0.65	1.45	2.4

The NCNT gas diffusion electrodes were assembled in a full electrochemical cell (see Figure S1 in the Supporting Information)[16] to examine their catalytic activity towards CO_2-reduction reaction (CRR). CO and $HCOO^-$ were observed as gas and liquid products, respectively, with CO as the major product (Figures S2 and S3). The trends in Faradaic efficiency (FE) for CO versus potential on various NCNT electrodes are shown in Figure 2a. NCNTs-ACN-850 exhibited the highest catalytic activity, with the highest maximum FE and lowest onset potential for CO formation. NCNTs-ACN-850 catalyzed CO formation at a potential as low as −0.7 V, reaching the maximum FE of about 80 % at −1.05 V, followed by a decreasing trend at more negative potentials. The decrease in FE at higher negative potentials stems from the dominance of the hydrogen-evolution reaction (HER) over the CRR.[11] The onset potential for CO formation over a NCNTs-ACN-850 electrode was also more anodic than the onset potentials observed for NCNTs-DMF-850 and NCNTs-TEA-850; that is, −0.8 V and −1.0 V, respectively. In addition, the maximum FE for CO reached about 80 % on the NCNTs-ACN-850 electrode compared to 25 % and 40 % for TEA- and DMF-derived NCNTs, respectively.

In order to compare the kinetics of CRR on various NCNTs, Tafel analysis was performed on the CO partial current density. A lower magnitude of the Tafel slope is desirable,[17] since this would indicate faster kinetics for CO formation. The Tafel slope for CO formation yielded the lowest value of 0.16 V dec^{-1} with NCNTs-ACN-850 (Figure 2b). A change in the Tafel slope with overpotential was observed for NCNTs-DMF-850 and NCNTs-TEA-850 electrodes. The Tafel slope increased from 0.23 to 1.67 V dec^{-1} as the magnitude of overpotential was increased from 0.25 to 1 V on NCNTs-DMF-850. On a similar trend, for the NCNTs-TEA-850, Tafel slope increased from 0.46 to 0.78 V dec^{-1} as the magnitude of overpotential was increased from 0.6 to 1.4 V. A change in surface coverage of adsorbed species could cause this change in the Tafel slope.[18] In addition, at higher applied cathode potentials, the presence of more water molecules inside the electrical double layer can hinder electron transfer to reactant species,[18b] resulting in higher values of Tafel slopes.

Despite the similar total nitrogen content in NCNTs-DMF-850 and NCNTs-TEA-850, the cata-

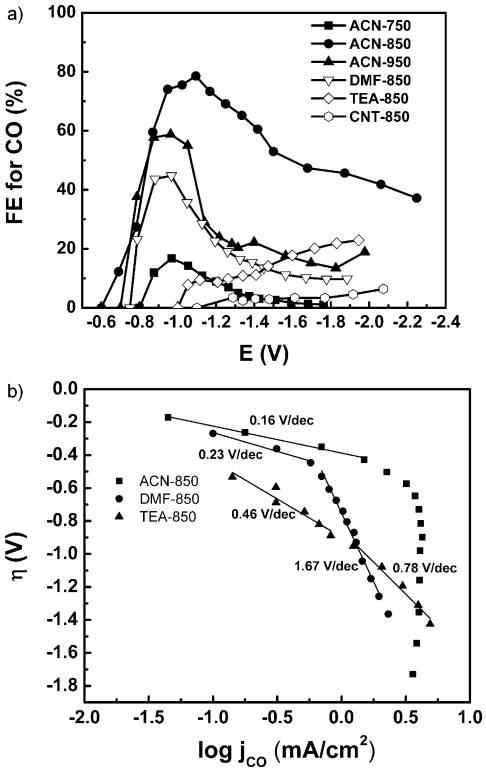

Figure 2. a) Faradaic efficiency for CO versus potential on NCNTs synthesized using different precursors and growth temperatures. ACN-750, ACN-850, and ACN-950 represent the NCNTs synthesized using the ACN precursor at 750, 850, and 950 °C, respectively. DMF-850 and TEA-850 denote the NCNTs synthesized using DMF and TEA precursors, respectively, at 850 °C, while CNT-850 represents the pristine CNTs synthesized using the benzene precursor at 850 °C. b) Tafel plots for CO formation on NCNTs synthesized using ACN, DMF, and TEA precursors at 850 °C.

lysts had remarkably different activities. We hypothesized that the difference in nitrogen moieties between the NCNTs is the origin of the disparity in the catalytic activity. The first verification of this hypothesis can be deduced from the comparison of activity between pristine CNTs and NCNTs electrodes. The selectivity (Faradaic efficiency) and overpotential in this work shows the independence on the electrochemical surface area. The CNTs exhibit a much lower selectivity and larger overpotential than NCNTs despite a greater electrochemical surface area listed in Table S1. The relationship between the nitrogen functionality content in NCNTs and the associated CRR activity is illustrated in Figure 3a. The figure shows that the catalytic activity descriptor of NCNTs, that is, the onset potential for CO formation has a positive correlation with the pyridinic and graphitic nitrogen contents. As the pyridinic and graphitic nitrogen contents increased in NCNTs from 0.3 to 1.1 at% and from 0.8 to 3.5 at%, respectively, the onset potential became more anodic, decreasing from −1.05 to −0.7 V. Following a similar trend, the maximum achievable FE for CO increased from about 14 to 80% as both pyridinic and graphitic N contents increased. This observation provides direct evidence that both pyridinic and graphitic N defects are active sites for CRR, eventually leading to the formation of

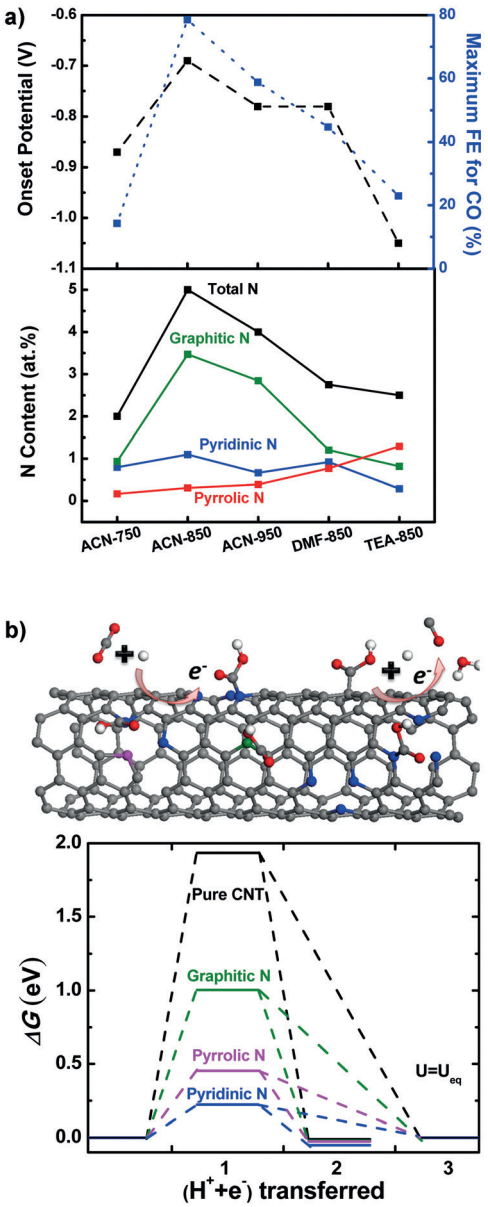

Figure 3. a) The onset potential and maximum Faradaic efficiency for CO formation as a function of N content in the synthesized NCNTs. b) Schematic illustrating CO formation on the NCNTs and free-energy diagram at equilibrium potential for CO_2 reduction on different N defects, that is, pyridinic, pyrrolic, and graphitic N in comparsion to pristine CNTs. C, O, and H atoms are represented by gray, red, and white spheres, while pyridinic, pyrrolic, and graphitic N defects are shown using blue, pink, and green spheres, respectively.

CO. However, the catalytic activity of pyridinic or graphitic nitrogen site alone cannot be distinguished based on our experimental data. This is also true for the case of the ORR, where the active site remains obscure between pyridinic and graphitic N defects.[7c,19] However, an increase in pyrrolic N content from 0.78 to 1.3 at% resulted in more cathodic onset potentials from −0.78 to −1.05 V. This cathodic shift in the onset potentials was also accompanied by a decrease in maximum achievable FE for CO from 40 to 25% upon increasing the pyrrolic N content, indicating a low activity for CRR at pyrrolic N defects. The higher catalytic activity of

NCNTs-DMF-850 compared to NCNTs-TEA-850 can be understood by the relatively high pyridinic N content of 0.9 at% in the NCNTs-DMF-850 to only 0.3 at% pyridinic N in the NCNTs-TEA-850.

The N-defect sites inside the graphitic carbon network facilitate the proton–electron pair transfers resulting in CO formation as shown in Figure 3b. DFT calculations predict the lowest absolute overpotential of 0.20 V for COOH*, an intermediate formed by the first coupled proton–electron transfer to CO_2 at a pyridinic N site, which eventually leads to CO formation.[11] Excess negative charge in the graphite basal plane is localized at the nitrogen atoms in the pyridine-like structure, resulting in its higher catalytic activity. Previous DFT work examining the ORR activity of NCNTs, has shown the wide disparity between the electronic density of states (DOS) for different nitrogen defect moieties. The DOS studies show that pyridinic defects retain a lone pair of electrons, which could bind CO_2. However, for graphitic-like nitrogen, electrons are located in the π* antibonding orbital, making them less accessible for CO_2 binding.[20] Although graphitic N exhibits a 1 eV higher barrier than pyridinic N for COOH* formation (Figure 3b), it still lowers the overpotential by 1 V in comparison to pristine CNTs, thus demonstrating significant activity. While pyrrolic defects have a nitrogen-based lone pair, the geometry of the defect moves the nitrogen atom towards the center of the tube making these electrons harder to access for CO_2 binding.[11] Furthermore, a careful inspection reveals that COOH* tends to bind to the adjacent pyridinic-like N site, instead of the pyrrolic N site, during the reduction process. Therefore, CRR is not promoted by only increasing pyrrolic N content, supporting our experimental observations.

In summary, NCNTs were synthesized with various surface structures and nitrogen contents by choosing different precursors (ACN, DMF, and TEA) and controlling the growth temperature. The catalytic activity of these NCNTs was found to depend upon the nature of nitrogen defects and defect density. The presence of graphitic and pyridinic N defects significantly decreases the absolute overpotential and increases the selectivity towards CO formation in comparison to pristine CNTs. NCNTs-ACN-850 exhibited the highest catalytic activity, that is, the lowest overpotential (ca. −0.18 V) and maximum selectivity (ca. 80% FE) owing to the highest pyridinic (ca. 1.1 at%) and graphitic N (ca. 3.5 at%) content. Furthermore, pyrrolic N defects seem to have little or no impact on CRR activity, which is congruent with DFT calculations.

Acknowledgements

This work is supported by the National Science Foundation under grant number DMR-1006113 and U.S. Air Force Office of Scientific Research 3D MURI (Award number: FA9550-12-1-0035). M.L. and B.I.Y. thank the support by the Office of Naval Research grant N00014-15-1-2251. R.M.Y. acknowledges the financial support from UGC India for Raman Fellowship under Indo-US 21st Century Knowledge Initiative.

Keywords: carbon dioxide fixation · carbon nanotubes · carbon monoxide selectivity · electrochemistry · nitrogen defects

How to cite: *Angew. Chem. Int. Ed.* **2015**, *54*, 13701–13705
Angew. Chem. **2015**, *127*, 13905–13909

[1] P. Friedlingstein, R. M. Andrew, J. Rogelj, G. P. Peters, J. G. Canadell, R. Knutti, G. Luderer, M. R. Raupach, M. Schaeffer, D. P. van Vuuren, C. Le Quere, *Nat. Geosci.* **2014**, *7*, 709–715.

[2] a) G. A. Olah, G. K. S. Prakash, A. Goeppert, *J. Am. Chem. Soc.* **2011**, *133*, 12881–12898; b) H. Arakawa, M. Aresta, J. N. Armor, M. A. Barteau, E. J. Beckman, A. T. Bell, J. E. Bercaw, C. Creutz, E. Dinjus, D. A. Dixon, K. Domen, D. L. DuBois, J. Eckert, E. Fujita, D. H. Gibson, W. A. Goddard, D. W. Goodman, J. Keller, G. J. Kubas, H. H. Kung, J. E. Lyons, L. E. Manzer, T. J. Marks, K. Morokuma, K. M. Nicholas, R. Periana, L. Que, J. Rostrup-Nielson, W. M. H. Sachtler, L. D. Schmidt, A. Sen, G. A. Somorjai, P. C. Stair, B. R. Stults, W. Tumas, *Chem. Rev.* **2001**, *101*, 953–996; c) J. Wu, F. G. Risalvato, S. Ma, X.-D. Zhou, *J. Mater. Chem. A* **2014**, *2*, 1647–1651.

[3] D. T. Whipple, P. J. A. Kenis, *J. Phys. Chem. Lett.* **2010**, *1*, 3451–3458.

[4] a) Y. Hori, H. Wakebe, T. Tsukamoto, O. Koga, *Electrochim. Acta* **1994**, *39*, 1833–1839; b) H. Noda, S. Ikeda, Y. Oda, K. Imai, M. Maeda, K. Ito, *Bull. Chem. Soc. Jpn.* **1990**, *63*, 2459–2462; c) J. Augustynski, P. Kedzierzawski, B. Jermann, in *Studies in Surface Science and Catalysis*, *Vol. 114* (Eds.: M. A. K. I. S. Y. T. Inui, T. Yamaguchi), Elsevier, Amsterdam, **1998**, pp. 107–116; d) J. J. Wu, F. G. Risalvato, F. S. Ke, P. J. Pellechia, X. D. Zhou, *J. Electrochem. Soc.* **2012**, *159*, F353–F359.

[5] K. Gong, F. Du, Z. Xia, M. Durstock, L. Dai, *Science* **2009**, *323*, 760–764.

[6] a) Y. Zheng, Y. Jiao, J. Chen, J. Liu, J. Liang, A. Du, W. Zhang, Z. Zhu, S. C. Smith, M. Jaroniec, G. Q. Lu, S. Z. Qiao, *J. Am. Chem. Soc.* **2011**, *133*, 20116–20119; b) R. Liu, D. Wu, X. Feng, K. Müllen, *Angew. Chem. Int. Ed.* **2010**, *49*, 2565–2569; *Angew. Chem.* **2010**, *122*, 2619–2623; c) Y. Li, W. Zhou, H. Wang, L. Xie, Y. Liang, F. Wei, J.-C. Idrobo, S. J. Pennycook, H. Dai, *Nat. Nanotechnol.* **2012**, *7*, 394–400; d) S. Wang, D. Yu, L. Dai, *J. Am. Chem. Soc.* **2011**, *133*, 5182–5185.

[7] a) S. Kundu, T. C. Nagaiah, W. Xia, Y. Wang, S. V. Dommele, J. H. Bitter, M. Santa, G. Grundmeier, M. Bron, W. Schuhmann, M. Muhler, *J. Phys. Chem. C* **2009**, *113*, 14302–14310; b) Z. Mo, S. Liao, Y. Zheng, Z. Fu, *Carbon* **2012**, *50*, 2620–2627; c) C. V. Rao, C. R. Cabrera, Y. Ishikawa, *J. Phys. Chem. Lett.* **2010**, *1*, 2622–2627.

[8] B. Kumar, M. Asadi, D. Pisasale, S. Sinha-Ray, B. A. Rosen, R. Haasch, J. Abiade, A. L. Yarin, A. Salehi-Khojin, *Nat. Commun.* **2013**, *4*, 2819.

[9] B. A. Rosen, A. Salehi-Khojin, M. R. Thorson, W. Zhu, D. T. Whipple, P. J. A. Kenis, R. I. Masel, *Science* **2011**, *334*, 643–644.

[10] S. Zhang, P. Kang, S. Ubnoske, M. K. Brennaman, N. Song, R. L. House, J. T. Glass, T. J. Meyer, *J. Am. Chem. Soc.* **2014**, *136*, 7845–7848.

[11] J. Wu, R. M. Yadav, M. Liu, P. P. Sharma, C. S. Tiwary, L. Ma, X. Zou, X.-D. Zhou, B. I. Yakobson, J. Lou, P. M. Ajayan, *ACS Nano* **2015**, *9*, 53645371.

[12] B. G. Sumpter, J. Huang, V. Meunier, J. M. Romo-Herrera, E. Cruz-Silva, H. Terrones, M. Terrones, *Int. J. Quantum Chem.* **2009**, *109*, 97–118.

[13] E. F. Antunes, A. O. Lobo, E. J. Corat, V. J. Trava-Airoldi, *Carbon* **2007**, *45*, 913–921.

[14] R. M. Yadav, J. Wu, R. Kochandra, L. Ma, C. S. Tiwary, L. Ge, G. Ye, R. Vajtai, J. Lou, P. M. Ajayan, *ACS Appl. Mater. Interfaces* **2015**, *7*, 11991.

[15] a) A. A. Koós, M. Dowling, K. Jurkschat, A. Crossley, N. Grobert, *Carbon* **2009**, *47*, 30–37; b) H. Liu, Y. Zhang, R. Li,

X. Sun, S. Désilets, H. Abou-Rachid, M. Jaidann, L.-S. Lussier, *Carbon* **2010**, *48*, 1498 – 1507.
[16] J. Wu, F. G. Risalvato, P. P. Sharma, P. J. Pellechia, F.-S. Ke, X.-D. Zhou, *J. Electrochem. Soc.* **2013**, *160*, F953 – F957.
[17] a) G. Ma, R. Jia, J. Zhao, Z. Wang, C. Song, S. Jia, Z. Zhu, *J. Phys. Chem. C* **2011**, *115*, 25148 – 25154; b) S. Zhong, L. Zhou, L. Wu, L. Tang, Q. He, J. Ahmed, *J. Power Sources* **2014**, *272*, 344 – 350.
[18] a) F. King, M. J. Quinn, C. D. Litke, *J. Electroanal. Chem.* **1995**, *385*, 45 – 55; b) C. C. Chang, T. C. Wen, *J. Appl. Electrochem.* **1997**, *27*, 355 – 363; c) L. Jiang, A. Hsu, D. Chu, R. Chen, *Int. J. Hydrogen Energy* **2010**, *35*, 365 – 372; d) S. Baranton, C. Coutanceau, E. Garnier, J. M. Léger, *J. Electroanal. Chem.* **2006**, *590*, 100 – 110; e) G. Wu, L. Li, B.-Q. Xu, *Electrochim. Acta* **2004**, *50*, 1 – 10.
[19] a) D. Deng, X. Pan, L. Yu, Y. Cui, Y. Jiang, J. Qi, W.-X. Li, Q. Fu, X. Ma, Q. Xue, G. Sun, X. Bao, *Chem. Mater.* **2011**, *23*, 1188 – 1193; b) L. Lai, J. R. Potts, D. Zhan, L. Wang, C. K. Poh, C. Tang, H. Gong, Z. Shen, J. Lin, R. S. Ruoff, *Energy Environ. Sci.* **2012**, *5*, 7936 – 7942; c) Z. Chen, D. Higgins, H. Tao, R. S. Hsu, Z. Chen, *J. Phys. Chem. C* **2009**, *113*, 21008 – 21013.
[20] S. Ni, Z. Li, J. Yang, *Nanoscale* **2012**, *4*, 1184 – 1189.

Received: July 2, 2015
Revised: September 1, 2015
Published online: September 25, 2015

